Ab Initio MO and TST Calculations for the Rate Constant of the HNO + $NO_2 \rightarrow$ HONO + NO Reaction

A. M. MEBEL,* M. C. LIN, K. MOROKUMA

Cherry L. Emerson Center for Scientific Computation and Department of Chemistry, Emory University, Atlanta, Georgia 30322

Received 29 September 1997; accepted 10 April 1998

ABSTRACT: Potential-energy surfaces for various channels of the HNO + NO_2 reaction have been studied at the G2M(RCC,MP2) level. The calculations show that direct hydrogen abstraction leading to the NO + *cis*-HONO products should be the most significant reaction mechanism. Based on TST calculations of the rate constant, this channel is predicted to have an activation energy of 6–7 kcal/mol and an A factor of ca. 10^{-11} cm^3 molecule^{-1} s^{-1} at ambient temperature. Direct H-abstraction giving NO + *trans*-HONO has a high barrier on PES and the formation of *trans*-HONO would rather occur by the addition/1,3-H shift mechanism via the $HN(O)NO_2$ intermediate or by the secondary isomerization of *cis*-HONO. The formation of NO + HNO_2 can take place by direct hydrogen transfer with the barrier of ca. 3 kcal/mol higher than that for the NO + *cis*-HONO channel. The formation of HNO_2 by oxygen abstraction is predicted to be the least significant reaction channel. The rate constant calculated in the temperature range 300–5000 K for the lowest energy path producing NO + *cis*-HONO gave rise to

$$k_a = 7.34 \cdot 10^{-20}\, T^{2.64} \exp(-2034/T)\ \text{cm}^3\ \text{molecule}^{-1}\ \text{s}^{-1}.$$

 Int J Chem Kinet 30: 729–736, 1998

INTRODUCTION

All four species involved in the title reaction are known to coexist in most H/N/O-systems. The reaction may be an important sink for NO_2 in the early stages of nitramine and nitrate ester combustion reactions, because HONO is chemically less reactive than either HNO or NO_2.

The rate constant for the reaction in either the forward or the reverse direction is not known experimentally or theoretically. The reaction is exothermic by more than 23 kcal/mole and, in principle, can take place by several direct and indirect abstraction mechanisms.

**Present address:* Institute of Atomic and Molecular Sciences, Academia Sinica, P.O. Box 23-166, Taipei, Taiwan
Correspondence to: M. C. Lin
Contract grant Sponsor: Office of Naval Research
Contract grant number: N00014-89-J-1949
Contract grant Sponsor: Air Force Office for Scientific Research
Contract grant number: AFOSR F49620-95-1-0182 CK-5430
 CCC 0538-8066/98/100729-08

Direct mechanism:

$$\mathrm{HNO + NO_2} \xrightarrow{a} \mathrm{NO + \textit{cis}\text{-HONO}}$$
$$\xrightarrow{b} \mathrm{NO + \textit{trans}\text{-HONO}}$$
$$\xrightarrow{c} \mathrm{NO + HNO_2}$$

Indirect mechanism:

$$\mathrm{HNO + NO_2} \xrightarrow{d} \mathrm{HN(O)NO_2} \longrightarrow \mathrm{NO + \textit{trans}\text{-HONO}}$$
$$\xrightarrow{e} \mathrm{HN(O)ONO} \longrightarrow \mathrm{HNO_2 + NO}$$

The objective of this study is to elucidate the mechanisms involved and to provide the absolute values of the rate constants for various product channels over a wide range of reaction conditions for computer simulation of nitramine and nitrate ester combustion reactions using high-level ab initio molecular orbital methods aided by statistical reaction rate theory calculations.

CALCULATION METHODS

The geometries of the reactants, products, intermediates, and transition states have been optimized using the hybrid density functional B3LYP method [1] with the 6-311G-(d,p) basis set [2]. Vibrational frequencies, calculated at the B3LYP/6-311G(d,p) level, have been used for the characterization of stationary points, zero-point energy (ZPE) correction, and transition-state theory (TST) computations of the reaction rate constants. All the stationary points have been positively identified for minimum (number of imaginary frequencies NIMAG = 0) or transition state (NIMAG = 1). All the energies quoted and discussed in the present article include the ZPE correction. In some cases discussed below, we used the MP2/6-311G(d,p) approach [3] for geometry optimization and for vibrational frequency calculations.

In order to obtain more reliable energies, we used the G2M(RCC,MP2) method [4]. The G2M(RCC,MP2) method is a modification of the Gaussian-2 [G2(MP2)] approach [5], by default it uses B3LYP/6-311G(d,p) optimized geometries and ZPE corrections and substitutes the QCISD(T)/6-311G(d,p) calculation of the original G2 scheme by the restricted open-shell coupled cluster [6] RCCSD(T)/6-311G(d,p) calculation. The method can also be used with the MP2/6-311G(d,p) geometries and frequencies where ZPE corrections are scaled by 0.95. The total energy in G2M(RCC,MP2) is calculated as follows [4]:

$$E[\mathrm{G2M(RCC,MP2)}] = E[\mathrm{RCCSD(T)/6\text{-}311G(d,p)}] + \Delta E(+3\mathrm{df2p}) + \Delta E(\mathrm{HLC}) + \mathrm{ZPE},$$

where

$$\Delta E(+3\mathrm{df2p}) = E[\mathrm{MP2/6\text{-}311+G(3df,2p)}] - E[\mathrm{MP2/6\text{-}311G(d,p)}]$$

and the empirical "higher level correction"

$$\Delta E(\mathrm{HLC}) = -5.25\mathrm{n}_\beta - 0.19\mathrm{n}_\alpha,$$

where n_α and n_β are the numbers of α and β valence electrons, respectively.

The GAUSSIAN 92/DFT [7] and MOLPRO 94 [8] programs were employed for the potential-energy surface computations.

RESULTS AND DISCUSSION

The reaction of HNO with NO_2, as alluded to in the introduction, can occur by various mechanisms. Abstraction of the H atom from HNO by NO_2 can lead to the *cis* or *trans*-isomer of HONO and to HNO_2. On the other hand, the N atom of HNO can form a bond with the nitrogen or oxygen atom of NO_2 leading to intermediates of the HN_2O_3 stoichiometry. Another possibility is the bond formation between the O atom of HNO and N or O of NO_2. However, we could not locate any stable species with the HNOONO or $HNONO_2$ structures and ruled out these reaction channels. The second mechanism is discussed in greater detail below. The optimized geometries of the reactants, products, intermediates, and transition states are shown in Figure 1. Their energies, calculated at various levels of theory, are collected in Table I. Figure 2 illustrates profiles of the potential energy surfaces (PES) of various channels of the HNO + NO_2 reaction.

Direct Hydrogen Abstraction

First, we consider the reaction channels proceeding by abstraction of the hydrogen atom from HNO by NO_2. If the H atom is abstracted by the oxygen atom, HONO is formed in either *cis* or *trans* conformation. **TS1** is the transition state leading from the reactants to *cis*-HONO + NO. **TS1** has an early character; the breaking NH bond is stretched by only 0.04 Å as compared to that in HNO, while the forming OH bond is still 0.70 Å longer than that in HONO. The early character of the transition state can be attributed to the exothermicity of the HNO + $NO_2 \rightarrow$ NO +

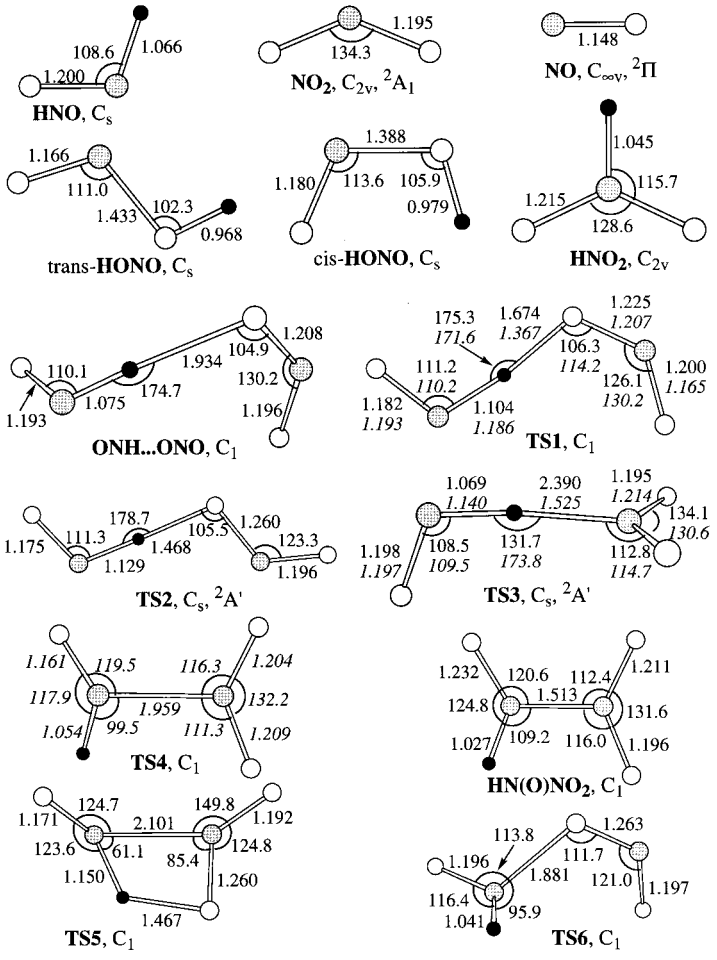

Figure 1 Optimized geometries of the reactants, products, intermediates, and transition states for the HNO + NO_2 reaction, calculated at the B3LYP/6-311G(d,p) level (bond lengths are in Å and bond angles are in degrees). For **TS1, TS3,** and **TS4,** italic numbers show the MP2/6-311G(d,p) optimized geometric parameters.

cis-HONO reaction, which is as high as 31.8 kcal/mol at the G2M(RCC,MP2) level. At the B3LYP level, the energy of **TS1** is slightly lower than that of HNO + NO_2 and the transition state actually connects a weak ONH . . . ONO complex with the products. The ONH . . . ONO complex (shown in Fig. 1) lies 0.4 kcal/mol below **TS1** at the B3LYP level without ZPE correction. At the G2M level, the energy of the complex formation from HNO and NO_2 is 2.2 kcal/mol. The B3LYP approach is known to underestimate barrier heights. Higher level calculations at the RCCSD(T)/6-311G(d,p) and G2M(RCC,MP2) levels give for the barrier at **TS1** the values of 6.4 and 5.3 kcal/mol, respectively.

For comparison, we also carried out geometry optimization of **TS1** at the MP2/6-311G(d,p) level. The geometry change from B3LYP to MP2 is significant; MP2 gives the NH distance 0.08 Å longer and HO 0.31 Å shorter than those at the B3LYP level, respectively. The barrier height for HNO + $NO_2 \rightarrow$ NO + *cis*-HONO at MP2/6-311G(d,p)//MP2/6-311G(d,p) is 22.7 kcal/mol. Using the MP2 optimized geometry we also performed a single point G2M(RCC,MP2) calculation and found that at the G2M(RCC,MP2)//MP2 level the barrier is 17.3 kcal/mol, close to the RCCSD(T)/6-311G(d,p)//MP2 value of 17.9 kcal/mol. The energy difference between the G2M(RCC,MP2)//B3LYP and G2M(RCC,MP2)//MP2 values is unexpectedly high, 12.0 kcal/mol. In order to reconcile these results, geometry optimization of **TS1** at higher theory levels, such as QCISD or CCSD, is required. At this stage, we believe that the B3LYP optimized geometry of **TS1** and, correspondingly, the G2M(RCC,MP2)//B3LYP energy are more accurate. This is based on comparison of the MP2, B3LYP, and QCISD optimized geometries of transition states for the H + O_2, O (^{3}P) + H_2, and N + O_2 reactions [4] as well as for H_2 + NO_2 [9]. The com-

Table I Relative Energies (kcal/mol) of Various Species Through the Reaction of HNO with NO_2 Optimized at the B3LYP/6-311G(d,p) Level of Theory

Species	UMP2/6-311G(d,p) ZPE[a]	UMP2/6-311G(d,p) E_{rel}	B3LYP/6-311G(d,p) ZPE	B3LYP/6-311G(d,p) E_{rel}	RCCSD(T)/6-311G(d,p)	UMP2/6-311+G(3df,2p)	G2M(RCC,MP2)
HNO + NO_2[b]	14.7	0.0	14.2	0.0	0.0	0.0	0.0
TS1, C_1		27.0	14.4	−2.3	6.4	25.8	5.3
TS2, C_s		48.0	13.9	5.0	21.5	47.2	20.6
TS3, C_s		−0.1	14.8	−0.4	0.2	−0.4	0.1
TS3 (MP2)[c], C_s	13.6	5.7		−1.9	8.0	6.0	8.2
TS4 (MP2)[c], C_1	17.1	21.6		−2.7	10.2	19.4	8.0
$HN(O)NO_2$, C_1		0.6	18.4	−12.0	−0.9	−3.0	−4.5
TS5, C_1		23.9	15.2	4.4	17.4	20.6	14.1
TS6, C_1		56.3	16.2	4.7	18.1	53.6	15.4
NO + *trans*-HONO	16.9	−25.1	15.9	−28.0	−31.8	−25.7	−32.1
NO + *cis*-HONO	17.0	−25.7	15.8	−28.2	−32.2	−25.5	−31.8
NO + HNO_2	18.4	−21.0	16.6	−19.1	−21.2	−21.4	−22.7

[a]ZPE is scaled by 0.95.

[b]The total energies of HNO + NO_2 are the following: UMP2/6-311G(d,p): −334.86877, B3LYP/6-311G(d,p): −335.64600, RCCSD(T)/6-311G(d,p): −334.90750, UMP2/6-311+G(3df,2p): −335.072347, G2M(RCC,MP2): −335.164788, including ZPE.

[c]Optimized at the MP2/6-311G(d,p) level.

parison clearly indicates that the B3LYP geometry in most cases closely agree with the QCISD one, while the MP2 geometry does not. Also, the MP2 approximation gives for **TS1** an unreasonably high imaginary frequency, 8631*i* cm^{-1}, which is an evidence of high spin contamination of the UMP2 wavefunction.

Transition state **TS2** connecting HNO + NO_2 with the NO + *trans*-HONO products has a much higher energy, 20.6 kcal/mol at the G2M level. The character of **TS2** is also early, but later than that of **TS1**. Although the *trans*-HONO is slightly more favorable energetically than *cis*-HONO, the former is significantly less reactive with respect to the hydrogen abstraction than the latter. Earlier, we observed the similar trend for the $NH_3 + NO_2 \rightarrow NH_2$ + *cis/trans*-HONO [10] and $H_2 + NO_2 \rightarrow H$ + *cis/trans*-HONO [9] reactions. In the reverse process, the barrier for abstraction of the hydrogen atom from *trans*-HONO is always higher than that from *cis*-HONO. We discussed this trend in detail earlier [10] and it was attributed to the repulsive interaction between an unpaired electron of NO_2 ($^2A_1$), located on the nitrogen p orbital directed outside of the ONO angle, and the forming O . . . H bond. The trend can be also explained using the concept of nodal lines. In the molecular plane of NO_2 the radical $6a_1^1$ orbital has two nodal planes, as shown below:

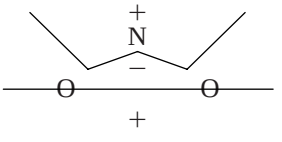

An approximately straight line through the two O atoms is one nodal plane. The second line is approximately the perpendicular bisector of the two NO bonds connected through the bonds. If the H of HNO attacks

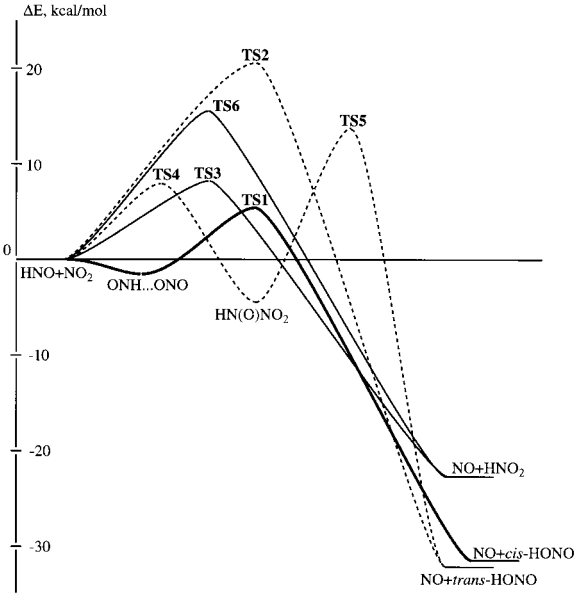

Figure 2 Profile of potential-energy surface (in kcal/mol) for the HNO + NO_2 reaction, calculated at the G2M(RCC,MP2) level.

NO_2 from below that corresponds to *cis*-HONO formation. There is sufficient room for the orbitals involved to not cross a nodal plane. If the H attacks from above, there is again room enough to produce the HNO_2 product without crossing a nodal plane. But if the H attacks from the side as needed for *trans*-HONO formation, it is interacting in the most confined region between nodal planes (and a region the calculations show has the most confined radical orbital extent). The result is that the nodal plane causes overlap cancellation and a significantly higher barrier. Because of the higher barrier at **TS2,** the reaction channel leading to NO + *trans*-HONO is not expected to compete with that producing NO + *cis*-HONO. We were unable to optimize geometry of **TS2** at the MP2 level; the energies are high and the transition state search does not converge.

A transition state for the HNO + $NO_2 \rightarrow$ NO + HNO_2 abstraction reaction also appeared difficult to calculate. At the B3LYP level, the optimized geometry of **TS3** represents the two reactants at a long separation from each other; the ONH . . . NO_2 distance is 2.39 Å. The energy of this structure is -0.4 and 0.1 kcal/mol relative to HNO + NO_2 at the B3LYP and G2M(RCC,MP2) levels, respectively. Apparently, in this case the B3LYP approximation fails to correctly reproduce the shape of PES and the transition-state position. Therefore, we reoptimized **TS3** using the MP2/6-311G(d,p) approach. At this level, the optimized structure looks more reasonable. The breaking NH and the forming OH bond lengths are 1.14 and 1.53 Å, respectively. Thus, the transition state exhibits an early character in accordance with the reaction exothermicity. The character of **TS3** is later than that of **TS1,** which is also in line with the Hammond rule; the NO + HNO_2 channel is less exothermic than NO + *cis*-HONO. Using the MP2 geometry of **TS3,** we calculated the barrier for the HNO + $NO_2 \rightarrow$ NO + HNO_2 abstraction reaction to be 8.2 kcal/mol at the G2M level, about 3 kcal/mol higher than the barrier for the HNO + $NO_2 \rightarrow$ NO + *cis*-HONO channel. The order of the barrier heights for the two channels corresponds to the order of their exothermicities. A similar trend was earlier found for the NH_3 + NO_2 hydrogen abstraction reaction, where the barrier eventually leading to the NH_2 + HNO_2 products is ca. 7 kcal/mol higher than the one leading to NH_2 + *cis*-HONO [10]. Since the UMP2 method is not the most reliable one for the calculations of geometries and, especially, vibrational frequencies of transition states for radical reactions and can suffer a severe spin contamination of the wavefunction [10–13], further studies would be required. In particular, geometry optimization and frequency calculations for **TS3** at a higher level, such as QCISD or CCSD, is needed but prohibitively time-consuming at present. We tentatively conclude that the NO + HNO_2 product channel has a higher barrier and is less significant for the HNO + NO_2 reaction than the NO + *cis*-HONO channel.

Indirect Hydrogen Transfer

The initial association of HNO with NO_2 can occur at either nitrogen or oxygen atom of the latter. First, we consider the reaction mechanism leading to a $HN(O)NO_2$ intermediate. $HN(O)NO_2$ has an asymmetric structure with a single NN bond. According to the calculated charge and spin density distribution, the dominant resonance structures are the following:

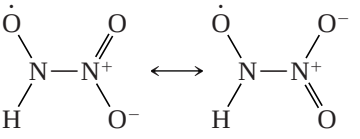

with the participation of

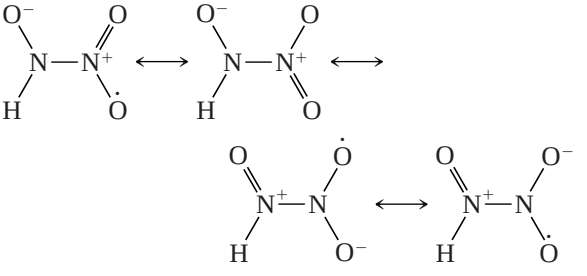

At the G2M level, $HN(O)NO_2$ lies 4.5 kcal/mol below the reactants.

Whether the barrier between HNO + NO_2 and $HN(O)NO_2$ exists, is a complicated question. At the B3LYP level, the search of the corresponding transition state was unsuccessful; the optimization always ends up in the reactants, HNO + NO_2, indicating that no barrier exists. On the other hand, the optimization at the MP2 level gives a transition state **TS4**. The G2M//MP2 calculated barrier is then 8.0 kcal/mol. This value is close to the barrier for the similar HNO + NO $\rightarrow$ HN(O)NO reaction, 9.5 kcal/mol [14]. A barrier of 5–6 kcal/mol was also found for the NN bond formation in the HNO + HNO reaction leading to HN(O)N(H)O [15]. On this basis, we believe that the MP26/6-311G(d,p) gives at least qualitatively correct geometry for **TS4**, and the G2M//MP2 calculated barrier is a reasonable estimate of the actual value. As for **TS3,** a further study of **TS4** including

its geometry optimization at the QCISD or CCSD level is also required.

After the $HN(O)NO_2$ intermediate is formed, the reaction can proceed by a 1,3-H shift from nitrogen to oxygen accompanied by splitting of the NN bond. The corresponding transition state is **TS5** and, after it is cleared, the NO + *trans*-HONO products are formed. The barrier at **TS5** is calculated to be 14.1 kcal/mol at the G2M//B3LYP level. Note that the geometries of $HN(O)NO_2$ and **TS5** do not differ significantly at the B3LYP and MP2 levels, and their G2M//B3LYP and G2M//MP2 energies agree within ca. 2 kcal/mol. The 1,3-hydrogen shift is the rate-determining step for the $HNO + NO_2 \rightarrow$ **TS4** $\rightarrow HN(O)NO_2 \rightarrow$ **TS5** $\rightarrow$ NO + *trans*-HONO reaction mechanism. The energy of **TS5** is 6.5 kcal/mol lower than that of **TS2,** so the formation of *trans*-HONO from $HNO + NO_2$ is more likely to occur by the addition/hydrogen shift mechanism than by direct hydrogen abstraction. On the other hand, *trans*-HONO can be formed in a secondary reaction of *cis*-HONO isomerization [16]. The reaction channel proceeding via the $HN(O)NO_2$ intermediate to NO + *trans*-HONO is expected to be less significant than $HNO + NO_2 \rightarrow$ **TS1** $\rightarrow$ NO + *cis*-HONO because of the higher barriers at **TS4** and **TS5**.

The second addition channel could proceed via a HN(O)ONO intermediate. However, at the B3LYP level no equilibrium structure with such geometry was found. Depending on the initial HN(O)-ONO distance, the optimization converges to either $HNO + NO_2$ or to HNO_2 + NO. A search of a HN(O)ONO-like transition state gives **TS6**. Intrinsic reaction coordinate (IRC) calculations [17] confirm that **TS6** connects the $HNO + NO_2$ reactants with the HNO_2 + NO products. The reaction is exothermic by 21.4 kcal/mol, and **TS6** is an early transition state. The forming NO bond is 1.88 Å, 0.67 Å longer than that in HNO_2, while the breaking ON bond is stretched by only 0.07 Å with respect to that in NO_2. Note that the B3LYP and MP2 optimized geometries of **TS6** are similar. Because of the high barrier at **TS6** (15.4 kcal/mol above the reactants), the $HNO + NO_2 \rightarrow HNO_2$ + NO channel proceeding by oxygen abstraction is expected to be the least significant one for the reaction. In particular, the barrier for oxygen abstraction is higher than the barrier for hydrogen abstraction at **TS3,** also leading to the HNO_2 + NO products.

Interestingly, the MP2 geometry optimization of HN(O)ONO shows that such an isomer may exist. At the G2M/MP2 level, it lies 6.0 kcal/mol higher than $HNO + NO_2$ and is separated from HNO_2 + NO by a low barrier of 3.5 kcal/mol (9.5 kcal/mol relative to $HNO + NO_2$). Apparently, at the B3LYP level, the barrier between HN(O)ONO and HNO_2 + NO disappears, and this isomer no longer exists. At both levels of theory, HN(O)ONO is not relevant to the reaction kinetics because this structure at best is a metastable intermediate which rapidly dissociates to HNO_2 + NO.

Rate Constants for the $HNO + NO_2 \leftrightarrow$ TS1 $\leftrightarrow$ NO + *cis*-HONO Reaction in the Forward and Reverse Directions

Because the direct hydrogen abstraction is expected to be the dominant reaction channel, we carried out TST calculations of the rate constant for this channel. We used the conventional method with Wigner's tunneling correction described earlier [10,13,18]. The molecular and transition state parameters of HNO, NO_2, **TS1,** NO, and *cis*-HONO calculated at the B3LYP level are shown in Table II. We calculated the rate constant by replacing the lowest frequency (60 cm^{-1}) with one-dimensional internal rotation. The lowest real frequency in **TS1** approximately corresponds to internal rotation around the N . . . H . . . O axis. Hence, we computed the reduced moment of inertia for the internal rotation based on the geometry of **TS1** and obtained the value of $26.94 \cdot 10^{-40}$ g cm^2 which was used in the rate constant calculations. The next two low frequencies, 87 and 126 cm^{-1}, correspond to

Table II Molecular and Transition-State Parameters of the Reactants, Products, and Transition States of the $HNO + NO_2$ Reaction, Used for the TST Calculations of the Rate Constants (Calculated at the B3LYP/6-311G(d,p) Level)

Species	i	I_i (10^{-40} g cm^2)	ν_j (cm^{-1})
HNO	A	1.521	1574, 1669, 2830
	B	19.72	
	C	21.24	
NO_2	A	3.606	767, 1394, 1701
	B	65.30	
	C	69.21	
TS1	A	74.64	183*i*, 60, 87, 126, 303,
	B	334.0	486, 765, 1205, 1475,
	C	382.5	1586, 1695, 2251
NO	A	0.0	1984
	B	16.49	
	C	16.49	
cis-HONO	A	10.07	665, 722, 945, 1338,
	B	63.24	1639, 3656
	C	73.36	

the in-plane (NH)O(NO) bending coupled with the ONHO torsion and the NHO bending coupled with the NHON torsion, respectively. The Arrhenius plot of the HNO + NO_2 → NO + *cis*-HONO rate constants is presented in Figure 3(a). The three-parameter fit in the 300–5000 K temperature range gives the following expression in cm^3 $molecule^{-1}$ s^{-1}:

$$k_a = 7.34 \cdot 10^{-20}\, T^{2.64} \exp(-2034/T)$$

No experimental data are available for comparison. The tunneling correction is found to be small because the imaginary frequency in **TS1** is as low as 183i cm^{-1}. The two-parameter fit for the 300–1000 K interval resulted in the following expression:

$$k_a = 1.85 \cdot 10^{-11} \exp(-6687/T)\ cm^3\ molecule^{-1}\ s^{-1}$$

The rate calculations using zero, one, or two internal rotors replacing none, one, or two lowest frequencies, respectively, gave quite similar results with the A factor varying from $5.8 \cdot 10^{-12}$ to $2.7 \cdot 10^{-11}$ and the activation energy in the 6.3–7.1 kcal/mol range. Thus, the ambient temperature activation energy for the HNO + NO_2 → NO + *cis*-HONO reaction is predicted to be 6–7 kcal/mol, while the A factor is ca. 10^{-11}.

Using the same approach, we calculated rate constants for the reverse NO + *cis*-HONO → HNO + NO_2 reaction which is endothermic by 31.8 kcal/mol and has a barrier of 37.1 kcal/mol. The Arrhenius plot is shown in Figure 3(b). The three-parameter expression in cm^3 $molecule^{-1}$ s^{-1} fitted for the 300–5000 K temperature range is:

$$k_{-a} = 3.59 \cdot 10^{-11}\, T^{-0.36} \exp(-19131/T)$$

The two-parameter fitting in the 300–1000 K temperature range gives an activation energy of 37–38 kcal/mol and an A factor of ca. 10^{-12}. The reverse reaction is much slower than the forward one.

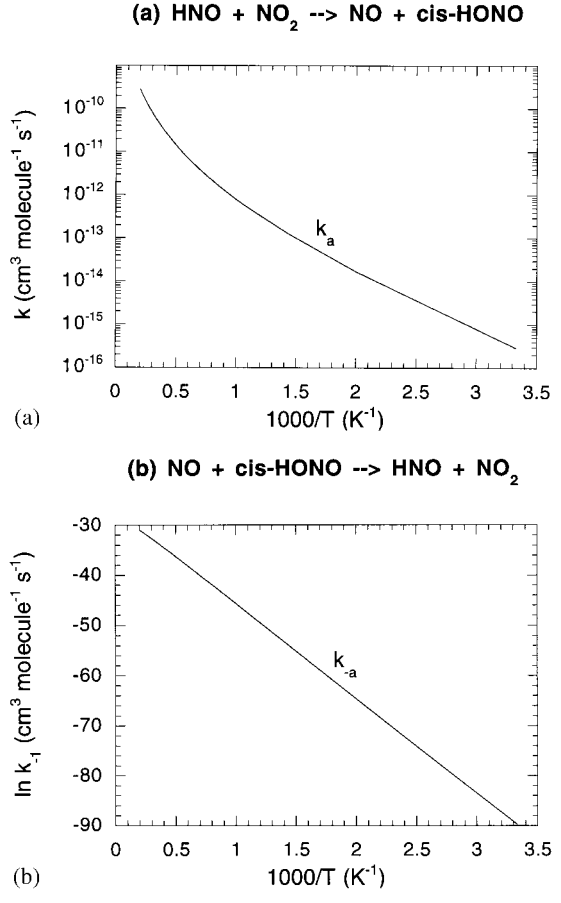

Figure 3 Arrhenius plots of the rate constants for the HNO + NO_2 ↔ NO + *cis*-HONO reaction in the forward (a) and reverse (b) directions.

CONCLUSION

We have studied potential energy surfaces for various channels of the HNO + NO_2 reaction. The calculations show that direct hydrogen abstraction leading to the NO + *cis*-HONO products via **TS1** should be the most significant reaction mechanism. Direct H-abstraction via **TS2** giving NO + *trans*-HONO has a high barrier on PES and the formation of *trans*-HONO would rather occur by the addition/1,3-H shift mechanism via the $HN(O)NO_2$ intermediate, HNO + NO_2 → **TS4** → $HN(O)NO_2$ → **TS5** → NO + *trans*-HONO, or by a secondary isomerization of *cis*-HONO. The formation of NO + HNO_2 can take place by direct hydrogen abstraction via **TS3.** We calculated the barrier at **TS3** to be ca. 3 kcal/mol higher than that at **TS1,** and the NO + HNO_2 channel is expected to be less important than NO + *cis*-HONO. However, since the B3LYP calculations of **TS3** have failed, more accurate calculations of this transition state are required to reliably predict the rate constant of the HNO + NO_2 → NO + HNO_2 channel. The formation of HNO_2 by oxygen abstraction via **TS6** is predicted to be the least significant reaction channel. TST calculations with tunneling correction have been performed for the major channel, HNO + NO_2 → **TS1** → NO + *cis*-HONO. At ambient temperature, the reaction is predicted to have an activation energy of 6–7 kcal/mol and an A factor of ca. 10^{-11} cm^3 $molecule^{-1}$ s^{-1}.

The authors gratefully acknowledge the support of this work by the Office of Naval Research (contract no. N00014-89-J-1949) under the direction of Dr. R. S. Miller and the Air Force Office for Scientific Research (grant no. AFOSR F49620-95-1-0182). We thank the Cherry L. Emerson Center for Scientific Computation for the use of computing facilities and various programs. Valuable comments of the referees are much appreciated.

BIBLIOGRAPHY

1. (a) A. D. Becke, *J. Chem. Phys.*, **98,** 5648 (1993); (b) C. Lee, W. Yang, and R. G. Parr, *Phys. Rev.*, **B37,** 785 (1988).
2. R. Krishnan, M. Frisch, and J. A. Pople, *J. Chem. Phys.*, **72,** 4244 (1988).
3. W. J. Hehre, L. Radom, P. v. R. Schleyer, and J. Pople, *Ab Initio Molecular Orbital Theory*, Wiley, New York, 1986.
4. A. M. Mebel, K. Morokuma, and M. C. Lin, *J. Chem. Phys.*, **103,** 7414 (1995).
5. L. A. Curtiss, K. Raghavachari, and J. A. Pople, *J. Chem. Phys.*, **98,** 1293 (1993).
6. (a) G. D. Purvis and R. J. Bartlett, *J. Chem. Phys.*, **76,** 1910 (1982); (b) C. Hampel, K. A. Peterson, and H.-J. Werner, *Chem. Phys. Lett.*, **190,** 1 (1992); (c) P. J. Knowles, C. Hampel, and H.-J. Werner, *J. Chem. Phys.*, **99,** 5219 (1994); (d) M. J. O. Deegan and P. J. Knowles, *Chem. Phys. Lett.*, **227,** 321 (1994).
7. M. J. Frisch, G. W. Trucks, M. Head-Gordon, P. M. W. Gill, M. W. Wong, J. B. Foresman, B. G. Johnson, H. B. Schlegel, M. A. Robb, E. S. Replogle, R. Gomperts, J. L. Andres, K. Raghavachari, J. S. Binkley, C. Gonzalez, R. L. Martin, D. J. Fox, D. J. DeFrees, J. Baker, J. J. P. Stewart, and J. A. Pople, GAUSSIAN 92/DFT (Gaussian, Inc., Pittsburgh, PA, 1993).
8. MOLPRO is a package of *ab initio* programs written by H.-J. Werner and P. J. Knowles, with contributions from J. Almlöf, R. D. Amos, M. J. O. Deegan, S. T. Elbert, C. Hampel, W. Meyer, K. Peterson, R. Pitzer, A. J. Stone, P. R. Taylor and R. Lindh.
9. C.-C. Hsu, M. C. Lin, A. M. Mebel, and C. F. Melius, *J. Phys. Chem.*, **A101,** 60 (1997).
10. A. M. Mebel, E. W. G. Diau, M. C. Lin, and K. Morokuma, *J. Phys. Chem.*, **100,** 7517 (1996).
11. F. Jensen, *Chem. Phys. Lett.*, **169,** 519 (1990).
12. A. M. Mebel, K. Morokuma, and M. C. Lin, *J. Chem. Phys.*, **101,** 3916 (1994).
13. A. M. Mebel, K. Morokuma, and M. C. Lin, *J. Chem. Phys.*, **103,** 3440 (1995).
14. A. M. Mebel, K. Morokuma, M. C. Lin, and C. F. Melius, *J. Phys. Chem.*, **99,** 1900 (1995).
15. A. M. Mebel, unpublished results.
16. J. M. Coffin and P. Pulay, *J. Phys. Chem.*, **95,** 118 (1991).
17. C. Gonzalez and B. H. Schlegel *J. Chem. Phys.*, **90,** 2154 (1989).
18. J. I. Steinfeld, J. S. Francisco, and W. L. Hase, Chemical Kinetics and Dynamics (Prentice-Hall, Englewood Cliffs, 1989).